EASR

Engineering and Applied Science Research

https://www.tci-thaijo.org/index.php/easr/index

Published by the Faculty of Engineering, Khon Kaen University, Thailand

Reduction and adsorption co-processes for selenate removal by zeolite-supported nanoscale zero-valent iron

Jakkapop Phanthasri[1)], Dickson Y.S. Yan[2)], Kitirote Wantala[3, 4)], Rattabal Khunphonoi[1, 4)] and Visanu Tanboonchuy*[1, 4)]

[1)]Department of Environmental Engineering, Faculty of Engineering, Khon Kaen University, Khon Kaen 40002, Thailand
[2)]Faculty of Science & Technology, The Technological and Higher Education Institute of Hong Kong, New Territories, Hong Kong
[3)]Department of Chemical Engineering, Faculty of Engineering, Khon Kaen University, Khon Kaen 40002, Thailand
[4)]Research Center for Environmental and Hazardous Substance Management (EHSM), Khon Kaen University, Khon Kaen 40002, Thailand

Received 1 March 2021
Revised 10 August 2021
Accepted 23 August 2021

Abstract

The removal of selenate (Se^{6+}) from aqueous solutions by zeolite Na-P1 supported nanoscale zero-valent iron (Z-NZVI) was investigated. Zeolite was synthesized from the fly ash of the byproducts discharged from coal-fired power, and used as supporting material for NZVI. The synthesized Z-NZVI was characterized using various techniques including x-ray diffraction (XRD), field emission scanning electron microscopy (FE-SEM), and BET surface area analysis, and. The results revealed that iron nanoparticles were highly dispersed on the zeolite surfaces which apparently lessened the agglomeration of iron nanoparticles resulting in the enhanced reduction process. The adsorption of Se^{6+} on Z-NZVI related well with Langmuir isotherm model with maximum adsorption capacity of 15.432 $mg \cdot g^{-1}$. The experimental results showed that the removal of Se^{6+} by Z-NZVI increased when the temperature increased. The reactions were found to conform to pseudo second order kinetics. The reaction process occurred spontaneously ($-\Delta G°$), in an endothermic process ($\Delta H°$=29.6 $J \cdot mol^{-1}$), and with increased randomness ($\Delta S°$=97.17 $J \cdot mol^{-1}K^{-1}$). This study suggested that Z-NZVI is a promising and efficient material for the selenate removal from wastewater.

Keywords: Selenate, Selenium, Fly ash, Zeolite, Nanoscale zero-valent iron, Adsorption

1. Introduction

Selenium (Se) is a hazardous pollutant to all living organisms. It causes serious environmental problems all over the world by both natural processes and human activities such as agricultural irrigation and drainage, coal-fired power plants, mining, and fossil fuels combustion [1]. World Health Organization (WHO) currently sets the maximum contaminant level (MCL) of Se in drinking water at 40 $\mu g \cdot L^{-1}$ [2]. In the aquatic environment, Se subsists in various forms depending on the oxidation state [3]. Selenate (SeO_4^{2-} or Se^{6+}), selenite (SeO_3^{2-} or Se^{4+}), selenium (Se^0), selenide (Se^{2-}), and organic selenium are found in different aquatic environments with common oxidation-reduction potential (ORP) and pH conditions [4]. The outstanding chemical forms Se^{6+} and Se^{4+} are mostly discovered aquatic zones [5]. While, Se^{6+} is more often found in groundwater [6]. Consequently, the oxidation states are very essential to determine and assess the potential methods for removing selenate from drainage water prior to discharge into the environment, which may causeSe^{6+} accumulation in the food chain.

Nanoscale zero-valent iron (NZVI) removes selenium from water via reduction of selenium oxyanions to elemental selenium. NZVI has gained great attention in recent years due to its high specific surface area, high reactivity, strong reduction potential, and low cost [7]. Many studies have been conducted on utilization of NZVI for groundwater remediation and wastewater treatment. Mokete et al. [8] found out that FeCu, FeNi and FeAg bimetals were synthesized by metal doping methods for phosphate removal. Maamoun et al. [9] studied a reactive material for permeable reactive barrier (PRB) technology for Cr (VI) removal from groundwater by nFe^0/Cu. Maamoun et al [10] indicated that effective phosphorus removal by iron-magnesium nanocomposite (nFe^0-Mg). Takami et al. [11] represented that developing a phosphorus removal system using NZVI particles in continuous system consisted of Continuous Stirred Flask Reactor (CSFR). However, one of the drawbacks associated with iron nanoparticles is related tothe rapid aggregation of the particles in water, which would significantly reduce its adsorption capacity [12]. In order to restrain further surface oxidation and prevent the iron particle agglomeration, supporting materials were used to support iron nanoparticles [13].

The most common parameters discussed when choosing the type of support materials are their high surface area and pore volume, biocompatibility, price, high exchange capacity, thermal and mechanical resistance [14-16]. In this aspect, zeolite was selected as a supporting material for NZVI. Synthesis of zeolites from fly ash are microporous, aluminosilicate minerals with three dimensional framework structures [17]. Zeolite is used to incorporate with iron ions, reducing ability of NZVI, and the composite also have synergetic effects due to the better dispersion of NZVI on zeolite. This will combine the strong reduction ability of NZVI with the high

*Corresponding author. Tel.: +66 4336 2140
Email address: visanu@kku.ac.th
doi: 10.14456/easr.2022.37

adsorption ability of zeolite, as well as better dissipation of iron nanoparticles on surface of zeolite which are expected to help improve the removal of Se^{6+} [18].

In this research, zeolite Na-P1 was employed as the support for iron nanoparticles to enhance the removal of Se^{6+} in wastewater.The zeolite supported nano zero-valent iron (Z-NZVI) integrated the advantages of reduction and adsorption process to efficiently remove Se^{6+}. The synthesized Z-NZVI was characterized by various techniques including X-ray Diffraction (XRD), field emission scanning electron microscopy (FE-SEM), and Brunauer-Emmett-Teller (BET) surface area analysis. Se^{6+} removal by Z-NZVI experiments were performed in a batch reactor at different temperatures to study kinetics, thermodynamic and isotherm models.

2. Materials and methods

2.1 Chemicals

Sodium selenate decahydrate ($Na_2SeO_4 \cdot 10H_2O$, Sigma-Aldrich), iron (II) sulfate heptahydrate ($FeSO_4 \cdot 7H_2O$, QReC), sodium hydroxide (NaOH, RCI Labscan), and sodium borohydride ($NaBH_4$, Loba Chemie Pvt. Ltd.). All chemicals used in this research are analytical reagent grade and used without further purification.

2.2 Preparation of the Z-NZVI synthesis

The zeolite (hereinafter referred to as Z) was synthesized by hydrothermal method as previously reported [19]. The Z-NZVI was prepared according to Li et al. [20]. Briefly, the mixture was made by dissolving 1 g of $FeSO_4 \cdot 7H_2O$ in 250 mL of de-ionized (DI) water and mixing with 0.75 g of Z under continuous stirring. 1 M HNO_3 was used to adjust the pH of the solution to 4, and the mixture was continuously stirred for 30 min at room temperature. Then, 25 mL of 1 M $NaBH_4$ solution was added at a rate of 1 mL·min^{-1} into the mixture under vigorous stirring to ensure the complete reduction of Fe^{2+}. The reaction can be written as equation (1).

$$Fe^{2+} + 2BH_4 + 6H_2O \rightarrow Fe^0 + 2B(OH)_3 + 7H_2 \uparrow \quad (1)$$

The black solid product of Z-NZVI was quickly washed several times with ethanol solution. The synthesized Z-NZVI were collected from the solution using a magnet, and dried in a vacuum dryer at 40°C for 24 h.

2.3 Characterizations of materials

The crystallographic structure and chemical composition were determined by X-ray diffraction (XRD, Bruker D8 Advance; Germany) with CuK_α radiation operated at 40 kV and 40 mA. The measurement were made in a range of 2Theta=10-50°, with 0.02°/step increment. Degree of crystallinity (DOC %) of the synthesized materials was calculated from the obtained XRD patterns as follows equation (2):

$$Crystallinity\ (\%) = \frac{Total\ area\ of\ crystalline\ peaks}{Total\ area\ of\ all\ peaks\ crystalline\ amorphous} x100 \quad (2)$$

$$D = \frac{K\lambda}{\beta cos\,\theta_B} \quad (3)$$

where D is the crystallite size, K is a Scherrer constant (0.9), λ is the wavelength of X-rays sources (CuK_α radiation, λ=0.1514 nm), β is the effective peak broadening taken as the full width at half maximum (FWHM) (in radians), and θ_B is Bragg's angle. The crystallite size of the particles was determined using the Scherrer equation (3). Field Emission Scanning Electron Microscopy (FE-SEM) (Carl Zeiss Model Auriga; Germany) was employed to examine the surface morphology of the materials. The specific surface area of the samples was determined on a Bel Sorp mini II specific surface area and pore size distribution analyzer (Japan) at 77 K with the Brunauer-Emmett-Teller method.

2.4 Batch experiments

2.4.1 Kinetic models

The experiments were conducted by the initial selenate concentration of 15 mg·L^{-1} with 1 g Z-NZVI. The pH of the system was measured using a pH and ORP meter, and adjusted by diluted solution of HNO_3 or NaOH. The residence time were set in a range of 0-90 min and the temperatures were varied at 303, 323, and 333 K. The concentrations of selenium were determined using an Inductively Coupled Plasma Optical Emission Spectroscopy (ICP-OES, Optima 8000; Perkin Elmer). Kinetic models have been proposed to understand the mechanism and to scale-up the efficiency of the adsorption process [21]. To investigate the potential rate reaction was determined by mathematical models such as pseudo first order, pseudo second order, and intraparticle diffusion kinetic models [22]. The linear form of pseudo first order equation based on solid capacity is generally expressed as follows:

$$\ln(q_e - q_t) = \ln q_e - k_1 t \quad (4)$$

where q_e and q_t are the amounts of selenate adsorption by Z-NZVI at equilibrium and at various time t (mg·g^{-1}); k_1 is the equilibrium rate constant of pseudo first order kinetics (min^{-1}).

The linear form of pseudo second order model based on solid phase adsorption is expressed as follows [23]:

$$\frac{t}{q_t} = \frac{1}{k_2 q_e^{\,2}} + \frac{t}{q_e} \quad (5)$$

where k_2 is the equilibrium rate constant of the pseudo second order kinetics ($g \cdot mg^{-1}min^{-1}$).

The intraparticle diffusion model explains the resistance of intraparticle diffusion affecting adsorption and is generally represented as follows

$$q_t = k_i t^{0.5} + c \tag{6}$$

where k_{id} is the intraparticle diffusion rete constant ($mg.g^{-1}min^{-0.5}$).

Kinetic experiments have been proposed to realize the mechanism, and to improve the efficiency of the reduction process [21], which can be written as the equation (7):

$$ln(\frac{C}{C_0}) = -k_{obs}t \tag{7}$$

when k_{obs} is the observed reaction rate constant (min^{-1}), the k_{obs} was calculated by the method of linear regression, approving calculation of the Arrhenius formula (E_a) to be expressed as follows equation (8) [24].

$$ln k_{obs} = -\frac{E_a}{RT} + ln A_0 \tag{8}$$

where the Arrhenius activation energy, E_a ($kJ \cdot mol^{-1}$) is determined by plotting k_{obs} versus temperature, and A_0 is the pre-exponential factor.

2.4.2 Thermodynamic parameters

The thermodynamic parameters including Gibbs free energy (ΔG°), enthalpy (ΔH°), and entropy (ΔS°) were calculated to evaluate the thermodynamic feasibility and the nature of the reaction process. ΔG° can be estimated from the following equations (9-11) [25]:

$$\Delta G^o = -RT ln k_d \tag{9}$$

Where R is the gas constant (8.314 $J \cdot mol^{-1} K^{-1}$); T is the temperature (K): and Equilibrium constant, k_d ($L \cdot g^{-1}$) is the thermodynamic equilibrium constant of the reaction process, which reflected selenate distribution between the solid and liquid phases at equilibrium. The k_d is calculated from equation (6):

$$k_d = q_e / C_e \tag{10}$$

According to the Van't Hoff equation (7):

$$ln k_d = \frac{\Delta S^o}{R} - \frac{\Delta H^o}{RT} \tag{11}$$

The values of ΔH° ($J \cdot mol^{-1}$) and ΔS° ($J \cdot mol^{-1}K^{-1}$) are calculated by the slope and intercept of the Van't Hoff plots [26].

2.4.3 Isotherm models

Adsorption isotherms were obtained by varying the initial selenium concentrations from 1 to 15 $mg \cdot L^{-1}$ in 50 mL vials with 0.1 g of Z-NZVI at pH 7 and 303 K. The samples were collected periodically over a period of 30 min under continuousmixing to quantify the initial and final selenium concentrations. Results of adsorption isotherms from the experiments were compared with Langmuir, Freundlich, and Dubinin-Radushkevitch isotherms [27] and isotherm models fitting was evaluated using R^2 values. Langmuir isotherm assumes that adsorption process is a monolayer adsorption of adsorbate onto a homogeneous surface of adsorbent. Langmuir isotherm can be described by the following equation (12-14).

$$q_e = \frac{q_m K_L C_e}{1 + K_L C_e} \tag{12}$$

where q_e and q_m are the amount of Se^{6+} uptake on the adsorbent at the equilibrium ($mg \cdot g^{-1}$) and at maximum adsorption capacity ($mg \cdot g^{-1}$), respectively. K_L is the rate constant of Langmuir isotherm, and C_e is the concentration of Se^{6+} at the equilibrium ($mg \cdot L^{-1}$). The equation can be rearranged find the values of q_m and K_L by linear regression method with graphical approach. Experimental data $1/q_e$ can be plotted as a function of $1/C_e$ as described by the equation (13).

$$\frac{1}{q_e} = \frac{1}{q_m K_L C_e} + \frac{1}{q_m} \tag{13}$$

Equilibrium parameter (R_L), defined as equation (14), where C_0 is initial Se^{6+} concentration 1-15 ($mg \cdot L^{-1}$) and K_L is the Langmuir's adsorption model constant ($L \cdot mg^{-1}$), was used to define whether the isotherm is unfavorable ($R_L > 1$), linear ($R_L = 1$), favorable ($0 < R_L < 1$) or irreversible ($R_L = 0$) [28].

$$R_L = \frac{1}{1 + K_L C_e} \tag{14}$$

Freundlich isotherm was based on the assumptions of multilayer adsorption of Se^{6+} onto heterogeneous surface of adsorbent with non-uniform distribution of heat of adsorption. Freundlich isotherm is described by the following equation (15-16).

$$q_e = K_F C_e^{\frac{1}{n}} \tag{15}$$

where K_F is the rate constant of Freundlich isotherm and n is the adsorption intensity. Equation (11) can be rearranged in the form of linear equation to find the value n and K_F using graphical method. ln q_e can be plotted as a function of C_e by the equation (16).

$$\ln q_e = \ln K_F + \frac{1}{n} C_e \tag{16}$$

Dubinin-Radushkevich isotherm describes the mechanism of adsorption of a physical adsorption or chemical adsorption. Dubinin-Radushkevich isotherm can be written in the equation (17-19) [29].

$$q_e = q_m e^{-\beta \varepsilon^2} \tag{17}$$

Equation (18) can be rearranged as:

$$\ln q_e = -\beta \varepsilon^2 + \ln q_m \tag{18}$$

where β is the rate constant of the energy absorption per quantity of adsorbent ($mol^2 \cdot J^{-2}$), and Ɛ is the Polanyi potential, determined by the following equation (19).

$$\varepsilon = RT \ln\left(1 + \frac{1}{C_e}\right) \tag{19}$$

when R is the gas constant ($J \cdot mol^{-1}K^{-1}$), and T is temperature (K). The free energy (E, $kJ \cdot mol^{-1}$) of sorption per molecule of adsorbent occur when Se^{6+} transposes to the surface of the solid in solution. It can be explained by the equation (20).

$$E = \frac{1}{\sqrt{2\beta}} \tag{20}$$

The adsorption energy (E) allows information with considered to the physical and chemical behavior of adsorption. If the value of E > 8 $kJ \cdot mol^{-1}$, the adsorption process offers that of the chemical adsorption, while for the values of E < 8 $kJ \cdot mol^{-1}$ proposes that the adsorption process is the physical adsorption [30].

2.4.4 Analysis of functional errors

Akaike's Information Criterion (AIC) is commonly statistical analysis. It was conducted in order to identify the best kinetic and isotherm models that represents the experimental results [31, 32]. The best fitted model to the experimental data has the lowest value of AIC, which is expressed as follows:

$$SSE = \sum_{i}^{N} (q_e^{exp} - q_e^{est})_i^2 \tag{21}$$

$$AIC = 2K + N \ln\left[\frac{SSE}{N}\right] + \frac{2K(K+1)}{N-K-1} \tag{22}$$

where the functional errors of the experimental (q_e^{exp}) and estimated (q_e^{est}), SSE is the sum of the squared errors based on adsorption capacities of materials, K is number of independently adjusted parameters in the applied model, N is number of experimental measurements, SSE is sum of the squared errors.

3. Results and discussion

3.1 Material characterization

The XRD patterns of fly ash (a), Z (b), NZVI (c), Z-NZVI (d), and spent Z-NZVI (e) are displayed in Figure 1. The XRD pattern of fly ash revealed Mullite and Hematite peaks which was consistent with previous studies [19]. The synthesized Z showed characteristic peaks of zeolite NaP1 according to JCPDS 39-0219 standard [33]. The XRD analysis confirmed the formation of NZVI with its outstanding peaks at 44.8° [34]. The XRD pattern of the synthesized Z-NZVI remained the major pattern of zeolite with the

addition peak at 2 Theta=30.1 degree referring to (220) planes, which corresponds to the characteristic peak of Fe_2O_3 [35]. This peak implied that the iron component in NZVI has been partly oxidized from Fe^0 to Fe^{3+} during preparation. In addition, the degree of crystallinity investigation revealed that crystallinity of the Z-NZVI was around 60.94%. The XRD data revealed average crystallity size of Z-NZVI as 44.138 nm. The XRD pattern of Z-NZVI after reaction with Se^{6+} in Figure 1(e) indicated that no obvious peaks, indicating the amorphous structure of $Fe(OH)_3$-Se [36].

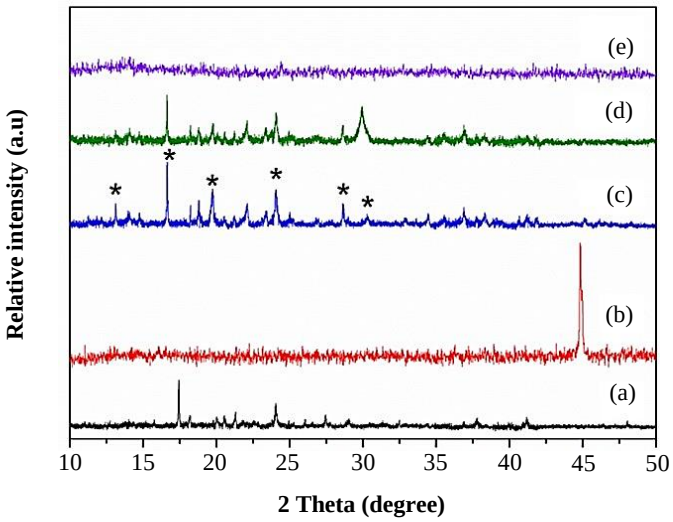

Figure 1 XRD Patterns of fly ash (a), Z (b), NZVI (c), fresh Z-NZVI (d), and spent Z-NZVI (e)

The SEM images of fly ash and Z are shown in Figure 2(a) and 2(b), respectively. The surface of Z appeared to be smooth although the amorphous alumino-silicates in fly ash were dissolved in alkaline solution, and formed sodium-silicate and allumino-silicate structure in Z. Figure 2(c) shows the change in morphology of the materials when iron nanpoparticles were deposited on the surface of zeolite. It can be seen that the NZVI particles were in spherical shape on Z surface with the average diameter of 109.45 nm. However, HR-TEM images of the NZVI was presented in our previous study [18]. The NZVI had spherical assemblages with strikingly uniform morphology and aggregated as chain-like clusters.

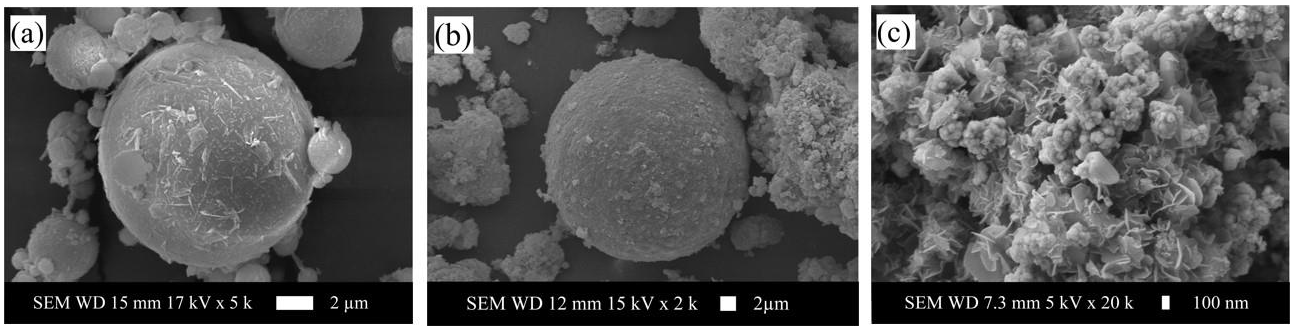

Figure 2 Field emission scanning electron microphotograph of fly ash (a), zeolite (b), and Z-NZVI (c) at magnification of 5 kX, 2 kX, and 20 kX, respectively

The surface area and pore structure of fly ash, Z, and Z-NZVI were studied by N_2 physical adsorption-desorption isotherms. Figure 3 shows N_2 adsorption-desorption isotherms and the relative Barret-JoynerHalender (BJH) pore size distributions received from the desorption branch of the isotherms of the adsorbents. Table 1 presen the specific surface area of fly ash, Z, and Z-NZVI determined by the Brunauer Emmett Teller (BET) procedure. The BET surface area of fly ash, Z, and Z-NZVI was 1.68, 35.60, and 61.72 $m^2 \cdot g^{-1}$, respectively. The improvement in surface area of Z-NZVI was due to the increased basal space of Z-NZVI. The isotherms of Z-NZVI in Figure 3(c) showed type IV isotherm with H3 hysteresis loops, indicating the mesoporous structure according to the IUPAC classifications [37]. From the BJH pore size distributions, the synthesized Z-NZVI possessed an average pore diameter and pore volume of 16.42 nm and 0.25 $cm^3 \cdot g^{-1}$, respectively. The increase in surface area of Z-NZVI was probably a result of the better distribution of iron nanoparticles when Z was used as the supporting material.

Table 1 BET Surface area of materials

Materials	BET surface area ($m^2 \cdot g^{-1}$)	Average pore diameter (nm)	Pore volume ($cm^3 \cdot g^{-1}$)
Fly ash	1.68	30.77	0.01
Zeolite	35.60	33.84	0.30
Z-NZVI	61.72	16.42	0.25

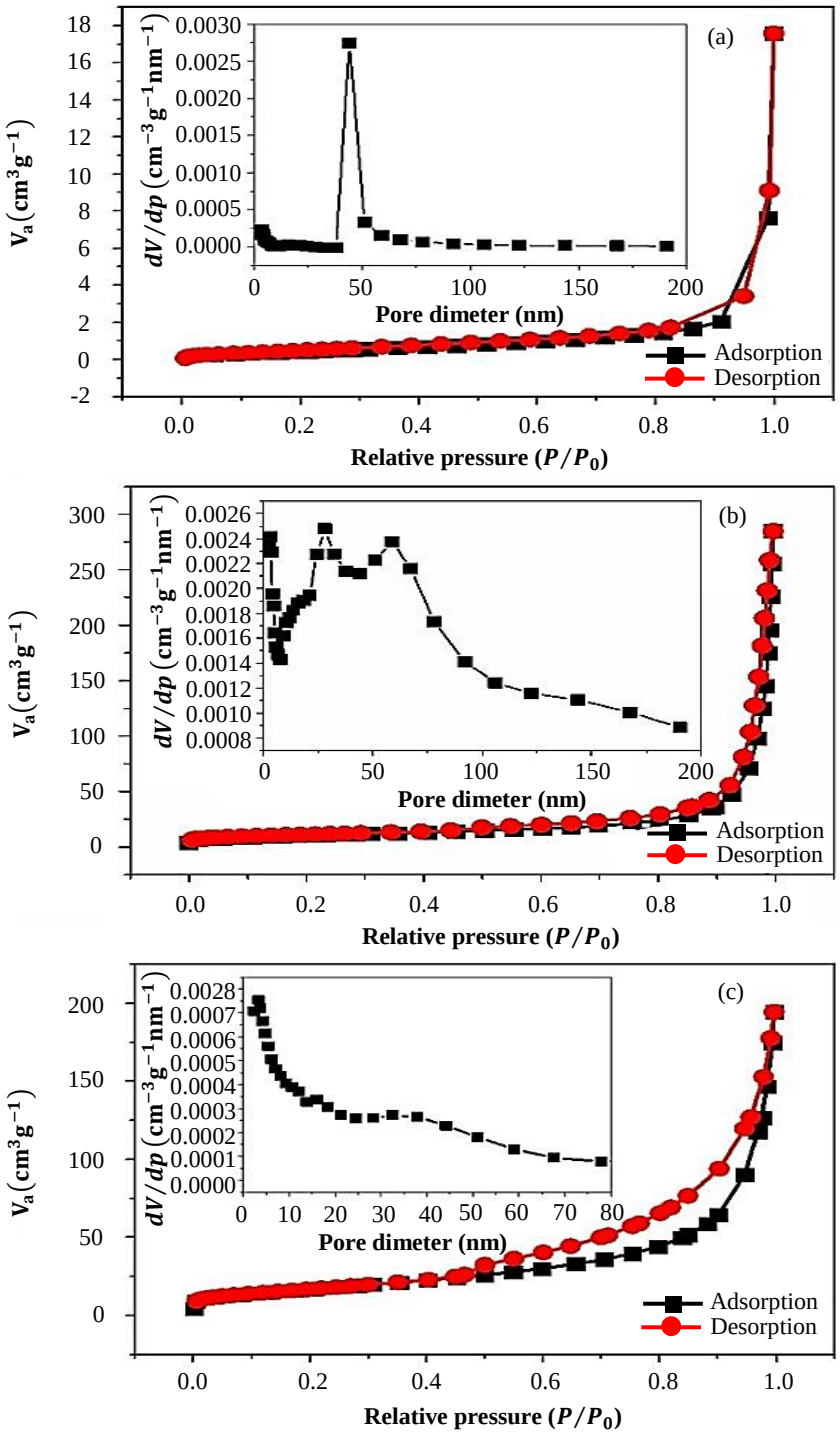

Figure 3 N_2 Adsorption-desorption BET isotherm for fly ash (a), zeolite (b), and Z-NZVI (c)

3.2 Kinetic and thermodynamic of selenate removing by Z-NZVI

The comparison of Se^{6+} removal by various reactive materials has been previously studied [18]. It indicated that the elimination of Se^{6+} by Z, NZVI, and Z-NZVI were about 0%, 70%, and 95%, respectively within 90 min. The removal efflciency of Se^{6+} using Z-NZVI at temperature of 303, 323, and 333 K are illustrated in Figure 4(a). The results showed that reaction capacity increased with increasing contact time and temperature. Slope and interception of the plotted linearized form in Figure 4(b) and 4(c) were respected to the calculation of the the kinetic parameters as shown in Table 2. It is indicated that a perfect agreement with the correlation parameter (R^2), where the pseudo second order kinetic model was the best selection for fitting with the experimental data corresponding to the lowest AIC values of -22.750, -15.867, and -16.977 at 303, 323, and 333 K, respectively. The pseudo second order kinetic model concluded that the rate kinetic reaction may strongly rely on the selenate concentration [38]. The E_a of Z-NZVI was obtained by using the Arrhenius formula and the value was 15.679 kJ·mol^{-1}. The result concluded that reduction reactions with E_a value in a range of 10-21 kJ·mol^{-1} has been considered that diffusion controlled and later changes to chemical control [39]. Figure 4(d) shows the intraparticle diffusion for the Se^{6+} adsorption into the Z-NZVI. None of the extrapolated lines passed through the origin, demonstrated that intraparticle diffusion was involved in the adsorption process [40]. The teperature of 333 K, the diffusion rate constants for external (ki_1) and internal (ki_2) mass transfer were found to be 1.4612 and 0.1446 mg·g^{-1}·min$^{-1/2}$, respectively.

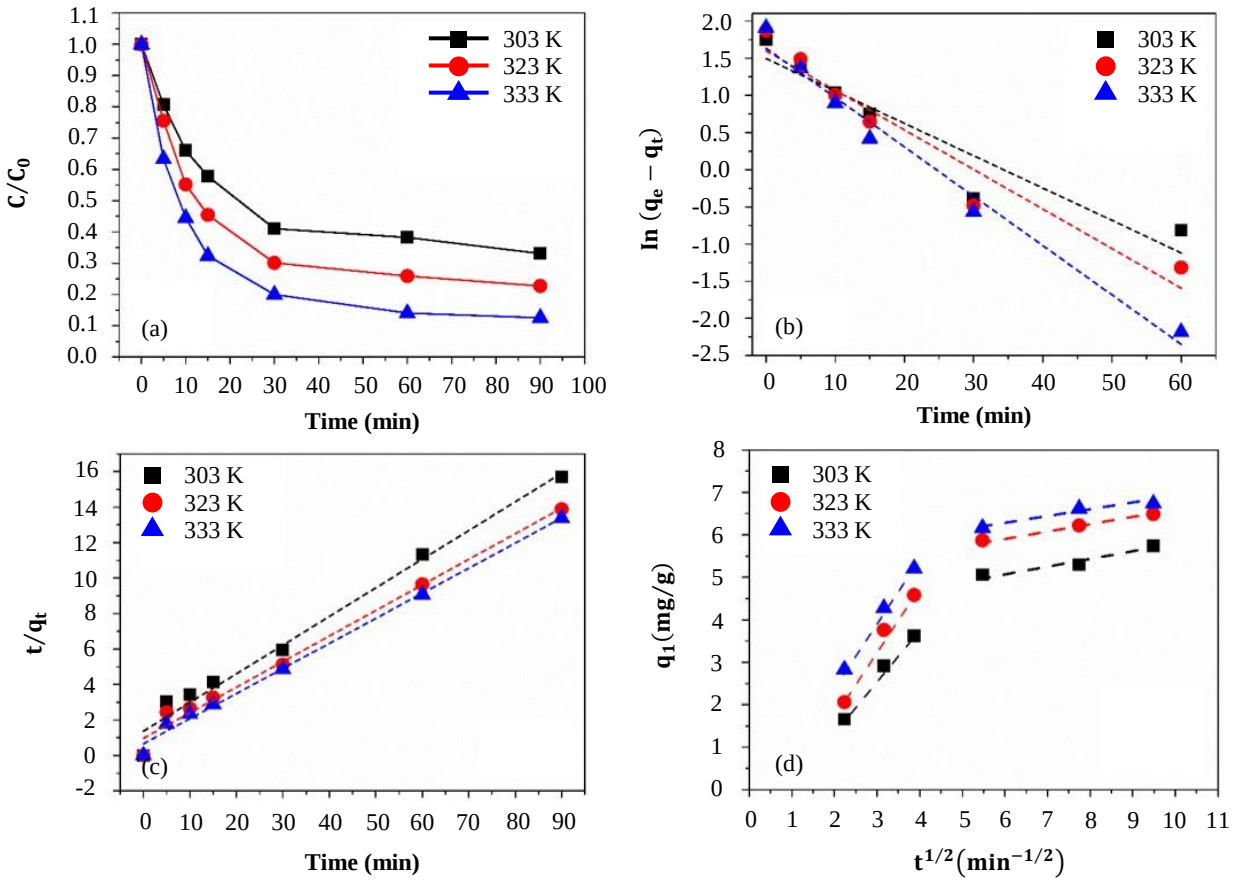

Figure 4 Kinetic parameters for Se^{6+} on Z-NZVI the concentration of Se^{6+} over a period of time (a), the pseudo first order kinetics model (b), the pseudo second order kinetics model (c), and intraparticle diffusion (d). (Condition: dosage= 2 $g \cdot L^{-1}$, initial Se^{6+}concentration of 15 $mg \cdot L^{-1}$, pH=7)

Table 2 Kinetic parameter of selenate removal by Z-NZVI.

T(K)	Pseudo first order					Pseudo second order			
	qe ($mg \cdot g^{-1}$)	k_1 (min^{-1})	q_1 ($mg \cdot g^{-1}$)	R^2	AIC values	k_2 ($g \cdot mg^{-1}min^{-1}$)	q_2 ($mg \cdot g^{-1}$)	R^2	AIC values
303	5.740	0.044	4.454	0.900	-0.73	0.022	5.945	0.959	-22.750
323	6.485	0.053	4.949	0.998	1.403	0.023	6.849	0.970	-15.867
333	6.730	0.066	5.125	0.982	1.928	0.030	7.062	0.986	-16.977

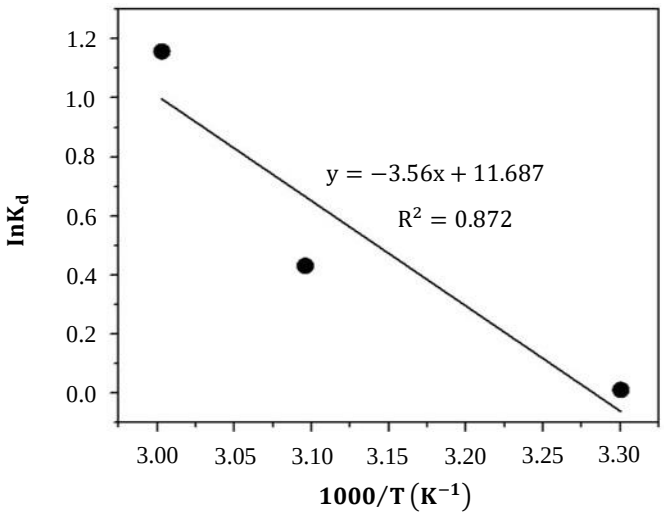

Figure 5 The relationship between lnk_d and 1000/T of selenate removal by Z-NZVI (Condition: dosage= 2 g L^{-1}, initial Se^{6+} concentration of 15 $mg \cdot L^{-1}$, pH=7)

The results of the thermodynamic calculations are shown in Figure 5 by the linear plot of lnk_d versus 1000/T, and the obtained thermodynamic parameters are presented in Table 3. The negative value for the Gibbs free energy (ΔG^o) indicated that the reaction processes were spontaneous in nature [41] and the degree of spontaneity of the reaction decreased with increasing temperatures

(303-333 K). The positive value of enthalpy change (ΔH^o=29.6 J·mol^{-1}) confirmed that the reaction process is endothermic. The values ΔH^o less than 40 kJ·mol^{-1} indicated that the adsorption was physisorption [25]. The positive value of entropy (randomness) (ΔS^o =97.17 J·mol^{-1}K^{-1}) also indicated an increased randomness at the interface of solid-liquid during the reaction [42].

Table 3 Thermodynamic parameters of Se^{6+} adsorption by Z-NZVI

T(K)	ΔG^o (kJ·mol^{-1})	ΔS^o (J·mol^{-1}K^{-1})	ΔH^o (J·mol^{-1})
303	-0.03		
323	-1.16	97.17	29.60
333	-3.20		

3.3 Isotherm modeling of selenate removing by Z-NZVI

Langmuir, Freundlich, and D-R isotherms were fitted with the experimental results and tabulated in Table 4. It is clear that the Langmuir model described the adsorption process best with high coefficient (R^2=0.993), compared to Freundlich isotherm (R^2=0.977) and D-R isotherm (R^2=0.737), in accordance to AIC values, Langmuir isotherm was the lowest compared with that of the other isotherm models. In addition, the presented curves tendencies for the Langmuir isotherms for Se^{6+} adsorption on Z-NZVI are nearly identical with experimemtals, presented in Figure 6. Thus, it indicated the monolayer coverage of Se^{6+} at the outside surface of Z-NZVI. The value maximum adsorption capacity (q_m) determined using Langmuir model was 15.432 mg Se^{6+} per g of Z-NZVI. The R_L values were in a range of 0.498-0.937, implying that the range of C_0=1-15 mg·L^{-1} is favorable for adsorption process. The adsorption energy obtained in this research was 1.279 J·mol^{-1}, suggesting that the process was physical adsorption. The results was in good agreement with the thermodynamic results [30]. Consequently, the mechanism of Se^{6+} contamination in aqueous solution by zeolite-supported nanoscale zero-valent iron, followed by fast reduction to Se^0 with Fe_2O_3 as the final corrosion product of Z-NZVI by co-precipitation according to previous studies [18]. Table 5 concludes the removal capacities of Se^{6+} with Z-NZVI, the maximum adsorption capacity of Z-NZVI is 15.43 (mg·g^{-1}). Consequently, the above discussion represented that Se^{6+} removal by zeolite-supported nanoscale zero-valent iron could be easily separated from the end water magnetically, it was a promising method compared to other literatures.

Table 4 Isotherm models parameters of adsorption capacity of adsorbents

Isotherms	Values
Langmuir model	
q_{max} (mg·g^{-1})	15.432
K_L (L·m·g^{-1})	0.033
R_L (C_0= 1-15 mg·L^{-1})	0.498-0.937
R^2	0.993
AIC values	9.041
Freundlich model	
K_F (mg·g^{-1})(L·mg^{-1})$^{1/n}$	0.928
n	0.927
R^2	0.977
AIC values	29.929
D-R isotherm model	
q_{max} (mg·g^{-1})	2.157
E (J·mol^{-1})	1.279
β (mmol^2·J^{-2})	0.306
R^2	0.737
AIC values	31.872

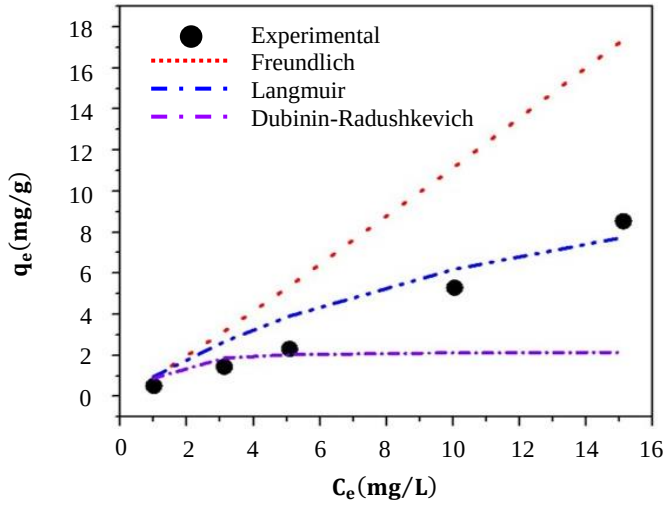

Figure 6 The adsorption isotherms for Se^{6+} removal on Z-NZVI. (Condition: dosage= 2 g·L^{-1}, temperature= 303 K, initial Se^{6+} concentration of 1-15 mg·L^{-1}, pH=7)

Table 5 Summary of Se^{6+} removal capacity with other adsorbents.

Adsorbents	pH	Initial [Se^{6+}] ($mg \cdot L^{-1}$)	Dosage of reductant ($g \cdot L^{-1}$)	Removal capacity ($mg \cdot g^{-1}$)	References
Z-NZVI	7.05	1-15	2.0	15.43	This study
ZVI	6.0	300.0	100.0	2.76	[43]
ZVI + Co^{2+}	6.2	20.0	Fe^0: 50 $g \cdot L^{-1}$, Co^{2+}: 59 mg L^{-1}	0.40	[44]
ZVI + Fe^{2+}	N.A.	20.0	Fe^0: 50 $g \cdot L^{-1}$, Fe^{2+}: 28 $mg \cdot L^{-1}$	0.40	[45]
Nano-NiFe	7.7	103.0	1.0	83.4	[46]
$MnFe_2O_4$	4.0	0.1	2.5	0.769	[1]
MGO	6.0	5.0	1.0	2.97	[47]
ZVI with WMF	6.0	100.0	1.0	36.9	[48]

MGO=magnetic nanoparticle-graphene oxide
WMF=weak magnetic field

4. Conclusions

This research indicated that Se^{6+} could be effectively removed by Z-NZVI. The morphology of Z-NZVI studied by FE-SEM showed that the aggregation of iron nanoparticles decreased when synthesis of zeolite from fly ash was used as the support. It helped increase the surface area of Z-NZVI, and thus the adsorption improved. The analysis of morphology revealed the spreading of the iron nanoparticles on the zeolite surfaces. The kinetic study showed that the reaction rate increased with increasing temperature. A study of thermodynamic parameters indicated that the reduction of Se^{6+} ions was spontaneous and endothermic. The experimental results for adsorption isotherm fitted well with the Langmuir isotherm model (R^2=0.993) and (the lowest AIC value) with the calculated maximum adsorption capacity of 15.432 mg Se^{6+} per g of Z-NZVI. The synthesized zeolite from fly ash suported with iron nanoparticles exhibited some unique features, such as small size, incresed surface area and excellent dispersibility which will significantly enhance their reactivity in the removal of selenate from aqueous solution**.** The findings in the research represented a bright future in the application of Z-NZVI by fixed-bed columns for Se^{6+} removal in contaminated wastewater.

5. Acknowledgements

This work was financially supported by the Electricity Generating Authority of Thailand (EGAT), Faculty of Engineering, Khon Kaen University, Research and Graduate Studies, Khon Kaen University, and Center of Excellence on Hazadous Substance Management (HSM), Patumwan, Bangkok, Thailand.

6. References

[1] Gonzalez CM, Hernandez J, Parsons JG, Gardea-Torresdey JL. A study of the removal of selenite and selenate from aqueous solutions using a magnetic iron/manganese oxide nanomaterial and ICP-MS. Microchem J. 2010;96(2):324-9.
[2] WHO. Guidelines for drinking water quality. 4th ed. Geneva: World Health Organization; 2011.
[3] Dev N, Hayes DF. Dynamics of selenium species in a wetland system of Great Salt Lake, Utah, USA. KKU Eng J. 2013;40(4):457-72.
[4] Tan G, Mao Y, Wang H, Junaid M, Xu N. Comparison of biochar- and activated carbon-supported zerovalent iron for the removal of Se(IV) and Se(VI): influence of pH, ionic strength, and natural organic matter. Environ Sci Pollut Res. 2019;26(21):21609-18.
[5] Sharrad M, Liu H, Fan M. Evaluation of FeOOH performance on selenium reduction. Separ Purif Tech. 2012;84:29-34.
[6] Ezzatahmadi N, Ayoko GA, Millar GJ, Speight R, Yan C, Li J, et al. Clay-supported nanoscale zero-valent iron composite materials for the remediation of contaminated aqueous solutions: a review. Chem Eng J. 2017;312:336-50.
[7] Dong H, Chen Y, Sheng G, Li J, Cao J, Li Z, et al. The roles of a pillared bentonite on enhancing Se(VI) removal by ZVI and the influence of co-existing solutes in groundwater. J Hazard Mater. 2016;304:306-12.
[8] Mokete R, Eljamal O, Sugihara Y. Exploration of the reactivity of nanoscale zero-valent iron (NZVI) associated nanoparticles in diverse experimental conditions. Chem Eng Process. 2020;150:107879.
[9] Maamoun I, Falyouna O, Eljamal R, Bensaida K, Eljamal O. Optimization modeling of nFe0/Cu-PRB Design for Cr(VI) removal from groundwater. Int J Environ Sci Dev. 2021;12(5):131-8.
[10] Maamoun I, Eljamal O, Falyouna O, Eljamal R, Sugihara Y. Stimulating effect of magnesium hydroxide on aqueous characteristics of iron nanocomposites. Water Sci Tech. 2019;80(10):1996-2002.
[11] Takami S, Eljamal O, Khalil AME, Eljamal R, Matsunaga N. Development of continuous system based on nanoscale zero valent iron particles for phosphorus removal. J Japan Soc Civ Eng. 2019;7(1):30-42.
[12] Sheng G, Hu J, Li H, Li J, Huang Y. Enhanced sequestration of Cr(VI) by nanoscale zero-valent iron supported on layered double hydroxide by batch and XAFS study. Chemosphere. 2016;148:227-32.
[13] Sun YP, Li XQ, Zhang WX, Wang HP. A method for the preparation of stable dispersion of zero-valent iron nanoparticles. Colloids Surf A Physicochem Eng Asp. 2007;308(1-3):60-6.
[14] Chen H, Cao Y, Wei E, Gong T, Xian Q. Facile synthesis of graphene nano zero-valent iron composites and their efficient removal of trichloronitromethane from drinking water. Chemosphere. 2016;146:32-9.
[15] Shubair T, Eljamal O, Tahara A, Sugihara Y, Matsunaga N. Preparation of new magnetic zeolite nanocomposites for removal of strontium from polluted waters. J Mol Liq. 2019;288:111026.
[16] Falyouna O, Eljamal O, Maamoun I, Tahara A, Sugihara Y. Magnetic zeolite synthesis for efficient removal of cesium in a lab-scale continuous treatment system. J Colloid Interface Sci. 2020;571:66-79.
[17] Yao G, Lei J, Zhang X, Sun Z, Zheng S, Komarneni S. Mechanism of zeolite X crystallization from diatomite. Mater Res Bull. 2018;107:132-8.

[18] Phanthasri J, Grisdanurak N, Khamdahsag P, Wantala K, Khunphonoi R, Wannapaiboon S, et al. Role of zeolite-supported nanoscale zero-valent iron in selenate removal. Water Air Soil Pollut. 2020;231(5):1-12.
[19] Chansiriwat W, Tanangteerapong D, Wantala K. Synthesis of zeolite from coal fly ash by hydrothermal method without adding alumina and silica sources: effect of aging temperature and time. Sains Malaysiana. 2016;45(11):1723-31.
[20] Li Z, Wang L, Meng J, Liu X, Xu J, Wang F, et al. Zeolite-supported nanoscale zero-valent iron: new findings on simultaneous adsorption of Cd(II), Pb(II), and As(III) in aqueous solution and soil. J Hazard Mater. 2018;344:1-11.
[21] Namasivayam C, Yamuna RT. Adsorption of chromium (VI) by a low-cost adsorbent: biogas residual slurry. Chemosphere. 1995;30(3):561-78.
[22] Soto ML, Moure A, Dominguez H, Parajo JC. Recovery, concentration and purification of phenolic compounds by adsorption: a review. J Food Eng. 2011;105(1):1-27.
[23] Ho Y, McKay G. Pseudo-second order model for sorption processes. Process Biochem. 1999;34(5):451-65.
[24] Chen ZX, Jin XY, Chen Z, Megharaj M, Naidu R. Removal of methyl orange from aqueous solution using bentonite-supported nanoscale zero-valent iron. J Colloid Interface Sci. 2011;363(2):601-7.
[25] Khan ZH, Gao M, Qiu W, Qaswar M, Islam MS, Song Z. The sorbed mechanisms of engineering magnetic biochar composites on arsenic in aqueous solution. Environ Sci Pollut Res. 2020;27(33):41361-71.
[26] Huang WY, Li D, Liu ZQ, Tao Q, Zhu Y, Yang J, et al. Kinetics, isotherm, thermodynamic, and adsorption mechanism studies of La(OH)3-modified exfoliated vermiculites as highly efficient phosphate adsorbents. Chem Eng J. 2014;236:191-201.
[27] Sheha RR, El-Shazly EA. Kinetics and equilibrium modeling of Se(IV) removal from aqueous solutions using metal oxides. Chem Eng J. 2010;160(1):63-71.
[28] Khandaker S, Toyohara Y, Saha GC, Awual MR, Kuba T. Development of synthetic zeolites from bio-slag for cesium adsorption: kinetic, isotherm and thermodynamic studies. J Water Process Eng. 2020;33:101055.
[29] Cruz-Olivares J, Perez-Alonso C, Barrera-Diaz C, Natividad R, Chaparro-Mercado MC. Thermodynamical and analytical evidence of lead ions chemisorption onto Pimenta dioica. Chem Eng J. 2011;166(3):814-21.
[30] Hallaji H, Keshtkar AR, Moosavian MA. A novel electrospun PVA/ZnO nanofiber adsorbent for U(VI), Cu(II) and Ni(II) removal from aqueous solution. J Taiwan Inst Chem Eng. 2015;46:109-18.
[31] Maamoun I, Eljamal R, Falyouna O, Bensaida K, Sugihara Y, Eljamal O. Insights into kinetics, isotherms and thermodynamics of phosphorus sorption onto nanoscale zero-valent iron. J Mol Liq. 2021;328:115402.
[32] Maamoun I, Eljamal O, Falyouna O, Eljamal R, Sugihara Y. Multi-objective optimization of permeable reactive barrier design for Cr(VI) removal from groundwater. Ecotoxicol Environ Saf. 2020;200:110773.
[33] Izidoro JDC, Fungaro DA, Dos Santos FS, Wang S. Characteristics of brazilian coal fly ashes and their synthesized zeolites. Fuel Process Tech. 2012;97:38-44.
[34] Eljamal R, Eljamal O, Maamoun I, Yilmaz G, Sugihara Y. Enhancing the characteristics and reactivity of nZVI: polymers effect and mechanisms. J Mol Liq. 2020;315:113714.
[35] Wang J, Liu G, Li T, Zhou C, Qi C. Zero-Valent iron nanoparticles (NZVI) supported by kaolinite for Cu(II) and Ni(II) Ion removal by adsorption: kinetics, thermodynamics, and mechanism. Aust J Chem. 2015;68(8):1305-15.
[36] Fu F, Lu J, Cheng Z, Tang B. Removal of selenite by zero-valent iron combined with ultrasound: Se(IV) concentration changes, Se(VI) generation, and reaction mechanism. Ultrason Sonochem. 2016;29:328-36.
[37] Sing KSW, Williams RT. Physisorption hysteresis loops and the characterization of nanoporous materials. Adsorpt Sci Tech. 2004;22(10):773-82.
[38] Ersali S, Hadadi V, Moradi O, Fakhri A. Pseudo-second-order kinetic equations for modeling adsorption systems for removal of ammonium ions using multi-walled carbon nanotube. J Nanostructure Chem. 2013;55(3):1-6.
[39] Geng B, Jin Z, Li T, Qi X. Kinetics of hexavalent chromium removal from water by chitosan-Fe0 nanoparticles. Chemosphere. 2009;75(6):825-30.
[40] Arancibia-Miranda N, Baltazar SE, Garcia A, Munoz-Lira D, Sepulveda P, Rubio MA, et al. Nanoscale zero valent supported by zeolite and montmorillonite: template effect of the removal of lead ion from an aqueous solution. J Hazard Mater. 2016;301:371-80.
[41] Kang YG, Yoon H, Lee W, Kim E ju, Chang YS. Comparative study of peroxide oxidants activated by nZVI: removal of 1,4-Dioxane and arsenic(III) in contaminated waters. Chem Eng J. 2018;334:2511-9.
[42] Al-Jubouri SM, Holmes SM. Hierarchically porous zeolite X composites for manganese ion-exchange and solidification: equilibrium isotherms, kinetic and thermodynamic studies. Chem Eng J. 2017;308:476-91.
[43] Gibson BD, Blowes DW, Lindsay MBJ, Ptacek CJ. Mechanistic investigations of Se(VI) treatment in anoxic groundwater using granular iron and organic carbon: an EXAFS study. J Hazard Mater. 2012;241-242:92-100.
[44] Tang C, Huang YH, Zeng H, Zhang Z. Promotion effect of Mn^{2+} and Co^{2+} on selenate reduction by zero-valent iron. Chem Eng J. 2014;244:97-104.
[45] Tang C, Huang YH, Zeng H, Zhang Z. Reductive removal of selenate by zero-valent iron: the roles of aqueous Fe^{2+} and corrosion products, and selenate removal mechanisms. Water Res. 2014;67:166-74.
[46] Mondal K, Jegadeesan G, Lalvani SB. Removal of selenate by Fe and NiFe nanosized particles. Ind Eng Chem Res. 2004;43(16):4922-34.
[47] Fu Y, Wang J, Liu Q, Zeng H. Water-dispersible magnetic nanoparticle-graphene oxide composites for selenium removal. Carbon. 2014;77:710-21.
[48] Liang L, Guan X, Huang Y, Ma J, Sun X, Qiao J, et al. Efficient selenate removal by zero-valent iron in the presence of weak magnetic field. Separ Purif Tech. 2015;156:1064-72.